Nanoemulsions Embedded in Alginate Beads as Bioadhesive Nanocomposites for Intestinal Delivery of the Anti-Inflammatory Drug Tofacitinib

Valentina Andretto, Giuseppe Taurino, Giulia Guerriero, Hanäé Guérin, Emmanuelle Lainé, Massimiliano G Bianchi, Géraldine Agusti, Stéphanie Briançon, Ovidio Bussolati, Alexandra Clayer-Montembault, et al.

pubs.acs.org/Biomac

Article

Nanoemulsions Embedded in Alginate Beads as Bioadhesive Nanocomposites for Intestinal Delivery of the Anti-Inflammatory Drug Tofacitinib

Valentina Andretto,[#] Giuseppe Taurino,[#] Giulia Guerriero, Hanäé Guérin, Emmanuelle Lainé, Massimiliano G. Bianchi, Géraldine Agusti, Stéphanie Briançon, Ovidio Bussolati, Alexandra Clayer-Montembault, and Giovanna Lollo*

Cite This: https://doi.org/10.1021/acs.biomac.3c00260

Read Online

ACCESS | Metrics & More | Article Recommendations | Supporting Information

ABSTRACT: Oral administration of nanoparticles (NPs) is a promising strategy to overcome solubility and stability issues of many active compounds. However, this route faces major obstacles related to the hostile gastrointestinal (GI) environment, which impairs the efficacy of orally administered nanomedicines. Here, we propose nanocomposites as a promising approach to increase the retention time of NPs in the intestinal tract by using bio- and mucoadhesive matrixes able to protect the cargo until it reaches the targeted area. A microfluidic-based approach has been applied for the production of tailored nanoemulsions (NEs) of about 110 nm, used for the encapsulation of small hydrophobic drugs such as the anti-inflammatory JAK-inhibitor tofacitinib. These NEs proved to be efficiently internalized into a mucus-secreting human intestinal monolayer of Caco-2/HT29-MTX cells and to deliver tofacitinib to subepithelial human THP-1 macrophage-like cells, reducing their inflammatory response. NEs were then successfully encapsulated into alginate hydrogel microbeads of around 300 μm, which were characterized by rheological experiments and dried to create a long-term stable system for pharmaceutical applications. Finally, *ex vivo* experiments on excised segments of rats' intestine proved the bioadhesive ability of NEs embedded in alginate hydrogels compared to free NEs, showing the advantage that this hybrid system can offer for the treatment of intestinal pathologies.

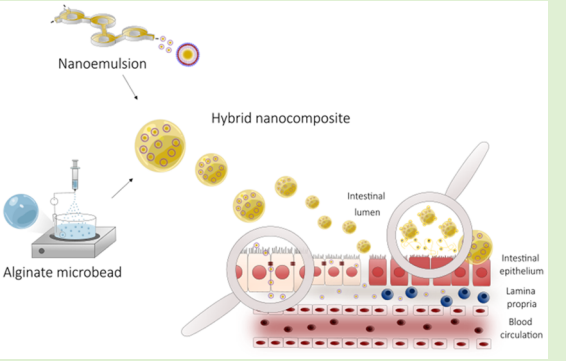

INTRODUCTION

The aim of drug delivery is to maximize therapeutic efficacy by carrying and releasing the active molecule to the target site in the body, thus minimizing off-target accumulation of the drug. Over the past decades, nanomedicine has enabled new approaches to address obstacles in the prevention and treatment of a number of human diseases.[1−4] However, one of the unsettled challenges in pharmaceutical technology is the design and complete characterization of a sustainable and targeted drug delivery system, specifically for poorly water-soluble or insoluble active compounds.[5] Nanocomposites based on the nanoparticle−hydrogel association represent a growing class of drug delivery systems composed of three-dimensional (3D) polymeric network embedding nanoparticles.[6] The main advantages of nanocomposites include modulated drug release kinetics by changes in the physiological environment, assisted site-specific drug targeting, and increased stability and drug loading.[7,8] In particular, innovative hybrid systems have recently been described as vehicles for active compounds in the human digestive tract.[9−11] Most of the nanocomposites administered orally are conceived to target intestinal inflammations while minimizing systemic effects, which still remains an unmet need in the treatment of intestinal inflammatory disorders such as IBDs (inflammatory bowel diseases).[12,13]

A wide variety of natural and synthetic polymers has been used, exploiting particular properties such as versatility and the opportunity to insert functionalities in a single structure. In particular, natural polymers such as alginates (AGs) represent attractive materials for biomedical applications.[14] AGs are naturally occurring biopolymers extracted from the cell walls of brown algae, currently used in an increasing number of applications in many medical areas.[15] They are linear, anionic polysaccharides composed of alternating blocks of α-1,4-L-guluronic acid (G) and β-1,4-D-mannuronic acid (M) units,

Received: March 13, 2023
Revised: May 10, 2023

with a M_w ranging between 10 and 600 kDa.[16] Their biocompatibility and biodegradability, together with their unique property to form stable gels in aqueous media under mild conditions, makes this biopolymer very useful for drug delivery. By interaction with divalent calcium cations (Ca^{2+}), AGs form hydrogels able to swell in answer to the environmental pH, thus allowing a targeted drug release at the intestinal level.[17] Alginates are classified as good bioadhesive agents,[18,19] and they may preferentially adhere to the inflamed parts of the intestinal tract, thanks to their overall negative charge that allows for a selective interaction with the exposed positively charged inflammatory proteins.[20,21] However, AG hydrogels alone have some limitations, such as low stability, which may facilitate premature degradation in the body and the consequent cargo release.[22] The incorporation of nanoparticles (NPs) into the AG matrix adds unique properties to the hydrogels, such as mechanical toughness, ability to adhere to surfaces, and responsiveness to external stimuli (irradiation, temperature, pH), which can modulate the release kinetics.

In this context, a hybrid nanocomposite was assembled from lipid-based NPs obtained through a microfluidic technology, and AGs have been conceived for the oral administration and localized delivery to an inflamed intestine.

A previously optimized mixture of lipids and surfactants was used for the formulation of nanoemulsions (NEs) able to form stable hybrid composites when mixed with different biopolymers.[23,24] To solve the lack of reproducibility and scalability limiting the clinical application of lipid-based NPs, we set up a technology transfer to microfluidic systems. As the drug candidate, the small hydrophobic molecule tofacitinib (TFC) was selected since it is already commercialized (Xeljanz) for the treatment of ulcerative colitis (UC)[25] and is currently in phase 2 clinical trial for the treatment of Crohn's disease (CD),[26] the two extreme phenotypes of IBDs. TFC is the first approved, reversible, and competitive inhibitor of Janus Kinases (JAK 1-2-3).[27] JAK activation follows the binding of several cytokines to their specific cell-surface receptors, which causes the phosphorylation of their cytoplasmic domains, providing docking sites for members of the signal transducer and activator of the transcription (STAT) protein family. In turn, these transcription factors induce the expression of several inflammatory mediators.[28] In IBDs, multiple proinflammatory cytokines are synthesized and secreted upon activation of the JAK-STAT pathway, leading to continuous activation of immune cells, thus contributing to the chronicity of inflammation. TFC prevents JAK activation and decreases cytokine production in the inflamed site, even though it can also cause systemic immune suppression.[29] Currently, orally administered TFC, formulated as an immediate-release film-coated tablet, is systemically absorbed to exploit its anti-inflammatory effects, accompanied by serious side effects.[30]

In the present work, the ability of the NEs to be internalized by the human intestinal epithelium to reach the immune cells in the *Lamina propria* was tested *in vitro* on a cell monolayer composed of Caco-2 and mucus-secreting HT29-MTX cells.[31] The anti-inflammatory inhibitory efficacy of the encapsulated drug on the JAK-STAT pathway was then verified with a triple co-culture made of THP-1 macrophage-like cells and the intestinal epithelial monolayer. To formulate a more suitable system for oral delivery, micron-sized carriers made of alginate hydrogels in the form of microbeads with entrapped NE were prepared. The single entities nano- and microsystems, as well as their combination in the form of hybrid nanocomposites were carefully characterized in terms of physicochemical, morphological, and mechanical properties. Furthermore, *in vitro* release and *ex vivo* bioadhesion studies on the intestine and colon of rats were also investigated.

EXPERIMENTAL SECTION (MATERIALS AND METHODS)

Materials. Medium-chain triglycerides, MCTs (Miglyol 812), were purchased from Cremer Oleo GmbH & Co. KG (Hamburg, Germany). Polyoxyethylene (40) stearate (Myrj 52), curcumin (CCM), phosphate-buffered saline (PBS) tablets (pH 7.4) were bought from Sigma Aldrich (St. Quentin-Fallavier, France). Oleoyl polyoxyl-6 glycerides (Labrafil M1944CS) were provided by Gattefossè (Saint-Priest, France). Tofacitinib (TFC) was purchased by CliniSciences (Nanterre, France). Methanol (HPLC grade), DiIC18(5) solid, 1,1′-dioctadecyl-3,3,3′,3′-tetramethylindodicarbocyanine, 4-chlorobenzene sulfonate salt (DiD), and sodium hydroxide were purchased from Thermo Fisher Scientific (Illkirch, France). Ethanol 96° was purchased from Carlo Erba Reagents (Val de Reuil, France). Milli-Q water was obtained using a Milli-Q academic system from Merck Millipore (Saint-Quentin-en-Yvelines, France). The aqueous phase used to prepare nanoemulsions (NEs) was PBS (pH 7.4). FaSSIF-V2 powders were purchased from Biorelevant (London, U.K.). Sodium chloride and hydrochloric acid were purchased from VWR International (Fontenay-sous-Bois, France). Sodium alginate was supplied by Alliance Gums & Industries (AGI, Cormeilles-en-Parisis). The alginate is harvested from brown seaweed. The percentage of mannuronic units in the alginate was close to 60%. The weight-average molecular weight (M_w) and the dispersity of the polymer were measured by a size-exclusion chromatography (SEC) system consisting of an Agilent 1260 system equipped with a differential refractometer Wyatt Optilab T-rEX (λ = 658 nm) and interfaced with a multiangle laser light scattering (MALS) detector (Wyatt HELEOS λ = 664 nm). The separation was carried out on two gel columns of PL aquagel OH mixed M and PL aquagel OH mixed H (300 mm × 7.5 mm, bead diameter: 8 μm). Elution was performed at 22 °C maintaining the flow rate at 0.5 mL/min. The eluent was sodium nitrate aqueous buffer (0.1 M) adjusted at pH 7.0 with sodium hydroxide solution. A refractive index increment (dn/dc) close to 0.13 was measured and used in data processing. The samples were prepared at a concentration of 1 mg/mL and filtered through a 0.45 μm pore-size membrane prior to injection. The values of M_w and the dispersity are 223 kg/mol and 1.6, respectively.

Formulation by the Microfluidic Technique and Physicochemical Characterization of Nanoemulsions. A NanoAssemblr Ignite system (Precision NanoSystems, Vancouver, Canada) was used to prepare oil-in-water (O/W) NEs. PBS 5 mM, pH 7.4 was used as a continuous aqueous phase. The dispersed, organic phase was an ethanolic solution containing the surfactants (mono-, di-, and triglycerides and PEG-6 (MW 300) mono- and diesters of oleic (C18:1) acid, and polyoxyethylene(40) stearate), and the oily phase Miglyol 812 N, consisting of medium-chain caprylic/capric acid triglycerides (MCTs). The amount of surfactants and oil in the organic phase was varied to obtain the highest possible lipid concentration, from 10 up to 50% w/v. The NE precursors were heated up to 60 °C to ensure complete homogenization prior to the addition of ethanol. The instrument parameters' total flow rate and flow rate ratio (aqueous/organic) were fixed at 10 mL/min and 3:1, respectively. Ethanol was removed by stirring the final system at room temperature over 24 h and then the samples were stored at 4 °C. TFC-loaded NEs were prepared by dissolving the drug in the organic phase at three different final concentrations: 2, 4, and 5.15 mg/mL. Similarly, DiD-loaded NEs (NE-DiD) were prepared by adding the carbocyanine derivative fluorescent dye in the organic phase to obtain a final concentration of 1.45 and 1.15 mg/mL for the *in vitro* assays and the *ex vivo* studies, respectively.

The size distribution and surface potential of the NE droplets were determined using a Malvern Zetasizer Nano ZS instrument (Malvern

https://doi.org/10.1021/acs.biomac.3c00260
Biomacromolecules XXXX, XXX, XXX−XXX

Instruments S.A., Worcestershire, U.K.). The particle sizes were measured by dynamic light scattering (DLS) at 25 °C at a scattering angle of 173°. The ζ-potential was calculated from the mean electrophoretic mobility measured for samples diluted in Milli-Q water. The stability of blank and drug-loaded NEs in a colloidal suspension was followed for 1 month upon storage at 4 °C. At scheduled time points, the particle size, polydispersity index (PDI), ζ-potential, and drug content were measured.

To quantify the TFC loaded in the nanosystem, NEs were dissolved in methanol to break the particles' structure and analyzed by RP-HPLC. The liquid chromatography system consists of a UHPLC ACQUITY Arc with a diode array detector (PDA), binary pump, and septum injection valve with a fixed 20 μL loop. The analyte was monitored at 254 nm. Chromatographic analyses were carried out on a Kinetex C18 column, 150 mm × 4.6 mm, particle size of 5 μm (Phenomenex, Torrance, CA). In order to elute the compound, a mixture of methanol and water in a ratio of 50:50% v/v was used, and the column temperature was set at 30 °C. The HPLC calibration curve was linear (R^2 = 0.99) in the concentration range of 20−100 μg/mL. The method was validated according to ICH Q2(R1) guidelines. Detection and quantification limits (LOD and LOQ) were 6.17 and 18.69 μg/mL, respectively. The diluted samples were filtered using a nylon filter 0.22 μm (Whatman GmbH, Dassel, Germany) before injection in the HPLC system. The drug concentration was followed for 6 months. The encapsulation efficiency (EE) was calculated following eq 1, as the ratio of the mass of TFC, detected by RP-HPLC in the NE, to the total mass weighed in the organic mixture prior to injection in the microfluidic system

$$\text{EE}\ (\%) = \frac{\text{mass of TFC in NE}}{\text{mass of TFC in OP}} \times 100 \quad (1)$$

where OP is the organic phase injected in the microfluidic system.

Drug loading (DL) was calculated as the ratio of the mass of TFC, detected by RP-HPLC in the NE, to the total mass of the NE, as reported in eq 2

$$\text{DL}\ (\%) = \frac{\text{mass of TFC in NE}}{\text{mass of NE}} \times 100 \quad (2)$$

DiD-loaded NEs were analyzed using a Tecan Infinite M1000 PRO plate reader (Tecan GmbH, Gronig, Austria). Sample preparation followed the same procedure reported above. 100 μL of samples was plated on a 96-well flat bottom plate (Corning, Arizona) and analyzed with an excitation wavelength at 644 nm and emission at 663 nm.

***In Vitro* Drug Release of TFC from NEs.** A dialysis membrane method was used to assess the drug release from the nanoscaled formulation in a simulated intestinal fluid in a fasted state at pH 6.5 (FaSSIF-V2, Biorelevant, U.K.). A mini dialysis system (Slide-A-Lyzer MINI Dialysis Devices, 3.5 kDa MWCO) containing 200 μL of TFC-loaded NEs was placed in 14 mL of release medium, under sink conditions and incubated at 37 °C under a stirring speed of 160 rpm. Drug-loaded NEs were removed from the dialysis medium at predetermined time intervals, and the total TFC content was determined by RP-HPLC. At each withdrawal, the volume was replaced by an equivalent amount of 5 mM PBS to avoid modifications in the exchange kinetics.

CELL CULTURE AND TREATMENTS

Caco-2/HT29-MTX Co-culture. Caco-2 cells, derived from a human colorectal carcinoma, were provided by ATCC, while HT29-MTX cells, which are human colon carcinoma-derived, mucin-secreting goblet cells, were kindly provided by Prof. Antonietta Baldi, University of Milan. Caco-2 cells were cultured in minimum essential medium (MEM, Corning), while HT29-MTX cells were grown in Dulbecco's modified Eagle's medium (DMEM, Corning) with high glucose (4.5 g/L) and 10 mM sodium pyruvate. Both media were supplemented with 10% of fetal bovine serum (FBS, Lonza Group), 4 mM glutamine (EuroClone), antibiotics (streptomycin 100 g/mL penicillin, 100 U/mL, Euroclone), and, in the case of DMEM for HT29 cells, with 10 mM HEPES (Sigma Aldrich). A mixed suspension of Caco-2 and HT29-MTX cells (7:3) was seeded in HT29 culture medium at a density of 25 × 10^4 cells/cm^2 into cell culture inserts with membrane filters (pore size 0.4 μm) for Falcon 24-well multitrays (Cat. N 3095, Becton, Dickinson & Company, NJ), and grown for 21 days at 5% CO_2 at 37 °C in water-saturated air at atmospheric oxygen until a tight monolayer was formed (trans-epithelial electrical resistance, TEER > 700 Ω·cm^2), with a medium replacement every 2 days. Then, 1 or 10 μg/mL NEs, containing the far-red fluorescent, lipophilic carbocyanine DiD (NE-DID) was added at the apical side of the monolayer, and cell viability, TEER, and NE internalization were evaluated at different experimental times, as indicated in the figure captions.

THP-1 Cells. The human acute monocytic leukemia THP-1 cell line was originally provided by the Cell Bank of the Istituto Zooprofilattico Sperimentale della Lombardia ed Emilia-Romagna (Brescia, Italy). Cells were cultured at 5% CO_2 at 37 °C in water-saturated air at atmospheric oxygen in high-glucose DMEM, supplemented with 4 mM glutamine, antibiotics, and 10% of FBS. For macrophage differentiation, THP-1 cells were pulsed with 80 nM phorbol 12-myristate 13-acetate (PMA; Sigma Aldrich) and, after 3 h, were centrifuged for 3 min at 300 rcf. The pellet was washed with PBS, further centrifuged, and resuspended in standard growth medium. Cells were seeded at a density of 1.5 × 10^5 cells/cm^2 and incubated at 5% CO_2 at 37 °C. After 48 h, differentiated cells were washed twice with PBS and incubated in standard growth medium in the absence or in the presence of TFC, TFC-loaded nanoemulsions (NE-TFC) at increasing concentrations of the drug (0−100 μM), or empty NE (NE-Blank), corresponding to the quantity of NE in the NE-TFC condition. After 48 h, cell viability was evaluated.

Co-culture of THP-1 and Caco-2/HT29-MTX Cells. After 21 days of incubation, the inserts hosting the monolayer of Caco-2/HT29-MTX cells were transferred into wells containing differentiated THP-1 cells. Apical and basolateral media were replaced with fresh DMEM, supplemented with 10% FBS, 4 mM glutamine, antibiotics, and 10 mM HEPES. Cells were incubated in the absence or in the presence of 10 μM TFC or NE-TFC or NE-Blank (90 μg/mL corresponding to the quantity of NE in the NE-TFC condition at 10 μM TFC) in the apical compartment. After 1 h, 100 ng/mL *Escherichia coli* lipopolysaccharide (LPS, strain O55:B5, Sigma Aldrich) and 20 ng/mL interferon-γ (INF-γ, R&D Systems, Inc.) were added to the basolateral medium to provide a proinflammatory stimulus to THP-1 cells. After 24 h, inserts were removed, basolateral media were collected to quantify secreted cytokines, and adherent THP-1 cells were used to evaluate gene and protein expression through the real-time polymerase chain reaction (PCR) and western blot, respectively. As an experimental control, differentiated THP-1 cells were maintained in monoculture and incubated in the absence or in the presence of the proinflammatory stimuli with or without TFC, NE-TFC, or NE-Blank.

Cell Viability. Cell viability was assessed with the resazurin method. Experimental medium was replaced with the standard growth medium of each cell line, supplemented with resazurin (final concentration 44 μM), but without FBS, and cells were incubated at 5% CO_2 at 37 °C. Resazurin is a blue, nonfluorescent dye, which is reduced by NADH-dependent enzymes to resorufin, a fluorescent pink dye, which is then

https://doi.org/10.1021/acs.biomac.3c00260
Biomacromolecules XXXX, XXX, XXX−XXX

released into the extracellular medium. After 3 h of incubation, fluorescence was measured at λ_{ex} of 515 nm and λ_{em} of 586 nm with a fluorometer (EnSpire multimode plate readers, Perkin Elmer). Cell viability was expressed as the percentage of the control, calculated through the following formula

$$\text{viability (\%)} = \frac{\text{fluorescence (treated well)}}{\text{fluorescence (untreated well)}} \times 100 \quad (3)$$

where "untreated well" is represented by control conditions, under which cells were cultured in standard growth medium in the absence of treatments.

TEER Measurement. TEER was measured using an epithelial voltmeter (EVOM, World Precision Instruments Inc., Sarasota, FL). Changes in TEER were calculated with the following equation

$$\text{TEER (\%)} = \frac{\text{final TEER treated}}{\text{final TEER control}} \times \frac{\text{initial TEER control}}{\text{initial TEER treated}} \times 100 \quad (4)$$

Data were expressed as % of the control, where cells were cultured in the absence of NEs.

Gene Expression with Real-Time-PCR. The total RNA of Caco-2 and HT29-MTX cells cultured alone or co-cultured and of differentiated THP-1 cells was isolated with a GeneJET RNA Purification kit (Thermo Fisher Scientific) and reverse transcribed with a RevertAid RT Reverse Transcription Kit (Thermo Fisher Scientific). For real-time qPCR, cDNA was amplified in a StepOne Real-Time PCR System (Applied Biosystems) employing a PowerUp SYBR Green Master Mix (Thermo Fisher Scientific) with 5 pmol of the primers, indicated in the Supporting information (Table S1). The reaction consisted of 35 cycles, including a denaturation step at 95 °C for 30 s, followed by separate annealing (30 s) and extension (30 s, 72 °C) steps. Fluorescence was monitored at the end of each extension step. A no-template, no-reverse-transcriptase control was included in each experiment. At the end of the amplification cycles, a melting curve analysis was performed. Data analysis was made according to the relative standard curve method, and gene expression was normalized to the expression of the housekeeping gene *RPL15*.[32]

Protein Expression with Western Blot. Differentiated THP-1 cells were washed once with PBS and lysed with 60 μL of Laemmli sample buffer (250 mM Tris−HCl, pH 6.8, 8% SDS, 40% glycerol, and 0.4 M DTT) previously diluted in RIPA lysis buffer (20 mM Tris−HCl (pH 7.5), 150 mM NaCl, 1 mM Na_2EDTA, 1 mM EGTA, 1% Triton, 2.5 mM sodium pyrophosphate, 1 mM β-glycerophosphate, 1 mM Na_3VO_4, 1 μg/mL leupeptin), supplemented with a cocktail of protease inhibitors (Complete, Mini, EDTA-free, Roche). For each experimental condition, a pool of extracts from two wells was used. Lysates were heated at 95 °C for 5 min, and proteins were quantified through the Lowry method. 20 μg of proteins was loaded on an 8% polyacrylamide gel for SDS-PAGE. After electrophoresis at constant 50 mA, proteins were transferred to PVDF membranes (Thermo Fisher Scientific) at 4 °C overnight at constant 30 V. Nonspecific binding sites were blocked through 1 h incubation in blocking solution (Roche), diluted in TBS-Tween. Membranes were then incubated at 4 °C overnight with the following primary antibodies diluted in 5% of BSA in TBS-Tween solution: anti-phospho-STAT1 (rabbit, monoclonal, 1:1000, Cell Signaling), anti-STAT1 (rabbit, polyclonal, 1:1000, Cell Signaling), and anti-tubulin (mouse, monoclonal, 1:5000, Sigma Aldrich). After washing, the membranes were exposed for 1 h at room temperature to the HRP-conjugated anti-mouse or anti-rabbit IgG antibody (Cell Signaling Technology), diluted 1:10,000 in blocking solution. Immunoreactivity was visualized with the Immobilon Western chemiluminescent HRP substrate (Millipore). The images were captured with an Invitrogen iBright FL1500 imaging system (Thermo Fisher Scientific). Protein expression was normalized for tubulin.

Cytokine Quantification. TNF-α and IL-6 were quantified via specific human ELISA kits (Invitrogen, Thermo Fisher Scientific), following the manufacturer's instructions.

Evaluation of DiD-Loaded NEs' Entry into Mucus-Secreting Cell Monolayers. Monolayers of Caco-2/HT29-MTX cells were cultured in the absence or in the presence of DiD-loaded NEs (NE-DiD), as described above. Cell monolayers grown on membrane filters were washed twice in ice-cold PBS and incubated for 20 min in paraformaldehyde (3.7% v/v). Fixed cells were washed twice in PBS, treated for 15 min with 0.3% Triton-X100 in PBS, washed again, and incubated for 30 min in a solution of 1% BSA in PBS to block nonspecific binding sites. For the experiments performed in the absence of NE-DiD, cell monolayers were then incubated overnight in the presence of the following primary antibodies diluted in 10% BSA in PBS: anti-claudin-7 (rabbit, polyclonal, 1:400, Cell Signaling), anti-MUC5AC (mouse, monoclonal, 1:300, Invitrogen). The day after, cells were washed twice with PBS and exposed for 1 h to the secondary antibodies Alexa Fluor 488 goat anti-mouse (λ_{ex} 488 nm, λ_{em} from 515 to 540 nm) and Alexa Fluor 543 goat anti-rabbit (λ_{ex} 543 nm, λ_{em} from 580 to 630 nm) for the detection of MUC5AC and claudin-7, respectively, in the presence of Hoechst 33258 (1 μg/mL, λ_{ex} 405 nm, λ_{em} from 420 to 504 nm) for nuclei counterstaining. For the experiments performed in the presence of NE-DiD (λ_{ex} 644 nm, λ_{em} from 663 to 812 nm), apical media were harvested (see below), and the treated monolayers were incubated for 1 h in the presence of Alexa Fluor 580 phalloidin (3U/mL, λ_{ex} 556 nm, λ_{em} from 568 to 624 nm) to visualize the actin cytoskeleton, and Hoechst 33258 to counterstain nuclei.

At the end of incubation, monolayers were further washed, and slides were mounted with a cover slide in Glycergel medium (DAKO, Santa Clara, CA) and observed with a CLSM system (Stellaris 5, Leica Microsystems, Wetzlar, Germany) using a Plan-Apo 63X oil immersion objective (NA 1.4).

The apical media, harvested before monolayer fixation, were used to quantify the amount of NE-DiD left after the incubation with cells, measuring the fluorescent signal of NE-DiD with a fluorimeter EnSpire multimode plate reader. A six-point standard calibration curve of NE-DiD was used, and data were expressed as μg/mL.

Preparation and Characterization of Empty Alginate Microbeads (AGμ) and Nanocomposites (AGμ-NEs). AGμ and AGμ-NE microbeads, with and without TFC, were prepared by ionotropic gelation. The day prior to preparation, a mixture of 20 mL of 1% alginate (w/v) and 5% nanoemulsion (v/v) solution in Milli-Q water was prepared and left under stirring at room temperature overnight to allow complete polymer dissolution. 200 mL of 0.1 M calcium chloride solution in Milli-Q water was prepared as gelation medium. Ionotropic gelation was performed using an Encapsulator B-395-Pro instrument (Büchi, Flawil, Switzer-

https://doi.org/10.1021/acs.biomac.3c00260
Biomacromolecules XXXX, XXX, XXX−XXX

land) configured with the following optimized parameters: 4.5 mL/min flow rate; 1400 V voltage; 1200 Hz frequency. The AG/NE mixture was added dropwise through a 200 μm single nozzle at room temperature into a calcium chloride bath under continuous stirring (300 rpm). The newly formed microbeads were left under stirring in the calcium bath for 15 min, washed with Milli-Q water, and sealed in plastic vials at 4 °C. The average diameter of moisturized microbeads was characterized by optical microscopy, with a Leica DM 2000 LED (Leica Microsystems, Wetzlar, 12 Germany) instrument, connected to a Leica-DFC3000G digital camera (Leica Microsystems, Wetzlar, Germany). Images of microbeads were taken with a magnification of 5× and were analyzed with ImageJ software. The average size of microbeads ± standard deviation was deduced from the diameter measurement of 30 different microbeads selected randomly.

Rheological Properties of AGμ and AGμ-NE Microbeads' Suspension. To measure the apparent viscosity of the samples, flow sweep tests were carried out using a rheometer AR 2000 (TA Instruments, Guyancourt, France) fitted with a 25 mm 4° cone-plate geometry. Approximately 0.5 g of each sample was added to the plate, and the gap was fixed at 116 μm. The temperature was set at 24 °C. All measurements were carried out applying successive shear rates ranging from 0.001 to 1000 s^{-1}. During the measurements, the geometry was covered with a solvent trap to maintain a wet environment avoiding water evaporation from the samples.

Dynamic rheological measurements (strain sweep tests and frequency sweep tests) were also performed using a rheometer ARES (TA Instruments, Guyancourt, France) fitted with a plate−plate geometry (25 mm diameter). The temperature was set at 24 °C. Strain sweep tests were performed to ensure that the apparent rheological moduli measurements were carried out within the linear viscoelastic (LVE) region. Then, apparent storage (G') and loss (G'') moduli were measured from a constant strain frequency sweep within frequency ranges of 100−0.05 rad/s. All measurements were performed in triplicate.

AGμ and AGμ-NE Drying Procedure and Dried System Characterization. NEs, empty and NE-loaded AG microbeads, with and without the TFC, were freeze-dried to enable their long-term storage. The freeze-drying process involves the removal of water or other solvents from a frozen product by sublimation, under vacuum, at low pressure and at low temperature. Samples of AGμ and drug-loaded AGμ-NEs were lyophilized in a Cryonext pilot freeze-dryer (Cryonext, Saint-Aunès, France). The freeze-drying methodology was as follows: freezing at −50 °C for 6 h in a freeze-dryer chamber; primary drying from −50 to 0 °C for 24 h; and secondary drying at 20 °C for 12 h. Finally, the vials were sealed with rubber caps and stored at room temperature.

The residual water content of the AG-based microbeads was evaluated by thermogravimetric analysis (TGA). TGA was carried out using a TG 209 F1 Libra thermogravimetric analyzer (Netzsch, Selb, Germany). Approximately 10 mg of dried samples were sealed in an aluminum crucible. The raw alginate powders, AGμ and AGμ-NE, with and without TFC, were analyzed. Under a helium (He) flow, samples were heated from 25 to 210 °C with a heating rate of 2 °C/min. The mass loss (%) of samples was recorded depending on the time.

Scanning electron microscopy (SEM) was performed on dried AG microbeads following lyophilization using an FEI Quanta 250 FEG microscope at the Centre Technologique des Microstructures (CTμ) of the University Lyon 1 (Villeurbanne, France). Samples were coated under vacuum by cathodic sputtering with copper and observed by a scanning electron microscope under an accelerating voltage of 15 kV.

To determine the drug content of the drug-loaded AGμ-NE, 10 mg of dried microbeads were placed in 0.5 mL of citrate buffer 0.2 M (pH = 7). The mixture was stirred until complete bead dissolution, diluted 1:2 with methanol, and filtered with a 0.45 μm nylon filter (Whatman GmbH, Dassel, Germany) to perform reversed-phase HPLC analysis, as detailed in the Formulation by the Microfluidic Technique and Physicochemical Characterization of Nanoemulsions section. The drug loading capacity was calculated according to the following equation

$$\text{LC}\ (\%) = \frac{\text{mass of TFC in AG } \mu}{\text{mass of AG } \mu} \times 100 \quad (5)$$

AGμ and AGμ-NE Stability and Drug Release in Simulated Intestinal Fluids. AGμ-NEs were rehydrated by the addition of intestinal fluids. FaSSIF-V2 was prepared at pH 6.5 with the addition of a $CaCl_2$ solution to reach a final calcium concentration of 0.6 mM.[11] The resuspension ability and the stability of AGμ and AGμ-NES in simulated intestinal fluids were evaluated by optical microscopy following the protocol described in Rheological Properties of AGμ and AGμ-NE Microbeads' Suspension section. Stability studies were carried out over a period of 7 days in triplicate. To this aim, 5 mg of dried microbeads were diluted in 1.5 mL of FaSSIF-V2 for each time point (0, 0.5, 1, 2, 3, 5, 8, 24, 32, 48, 72, 144, and 168 h). All samples were incubated at 37 °C under horizontal shaking at 70 rpm using a Promax 1020 instrument and an Incubator 1000 (Heidolph, Instruments, Schwabach, Germany).

At each time point, a small amount of microbeads were collected for the determination of the average diameter by ImageJ software. In addition, the diameter gain percentage was measured by comparing the size of the AGμ at the precise time point, with the size before drying, according to the following equation

$$\text{diameter gain}\ (\%) = \frac{\text{size}(t) - \text{size before drying}}{\text{size before drying}} \times 100 \quad (6)$$

In parallel, the total volume of simulated buffer (1.5 mL) was carefully withdrawn and filtered using a 0.45 μm nylon syringe filter at each time point. The total TFC content was determined by RP-HPLC analysis, as described above. The size distribution of the TFC-loaded NEs released in the collected buffers over time was assessed by DLS analysis to evaluate the released NE integrity.

Mucoadhesion *Ex Vivo* Experiments. A mucoadhesion study of AGμ-NEs containing DiD for fluorescence detection was investigated on rat jejunum and colon mucosa, following a previously described protocol.[33] Water solution containing the tracer was used as a negative reference of mucoadhesion. Animal protocols were approved by the Committee for Ethical Issues, CEMEA Auvergne (Clermont-Ferrand, France). Briefly, tissue from the jejunum or colon (5 cm length) was taken, flushed with normal saline (0.9% NaCl) to remove the unbound mucus on the mucosal side, and cut open longitudinally. The tissue was mounted on a plastic support at an angle of 45° and washed with normal saline. 125 μL of

https://doi.org/10.1021/acs.biomac.3c00260
Biomacromolecules XXXX, XXX, XXX−XXX

Table 1. Physicochemical Properties of NEs, the Encapsulation Efficiency, and Drug Loading of the Formulations[a]

	TFC conc. (mg/mL)	Z-average (nm)	PDI	ζ-potential (mV)	TFC EE%	TFC DL%
NEs		113.3 ± 1.8	0.17 ± 0.05	−16.3 ± 0.1		
TFC-loaded NEs	2	111.5 ± 2.4	0.16 ± 0.09	−17.2 ± 0.6	73.3 ± 9.7	0.9 ± 0.1
	4	111.0 ± 2.4	0.17 ± 0.02	−13.6 ± 0.9	79.8 ± 5.1	2.0 ± 0.1
	5.15	112.3 ± 4.3	0.20 ± 0.03	−12.3 ± 0.4	83.9 ± 5.9	2.7 ± 0.2
DiD-loaded NEs		112.0 ± 0.9	0.15 ± 0.02	−12.9 ± 0.3		

[a]Data are expressed as the mean ± standard deviation (n = 3).

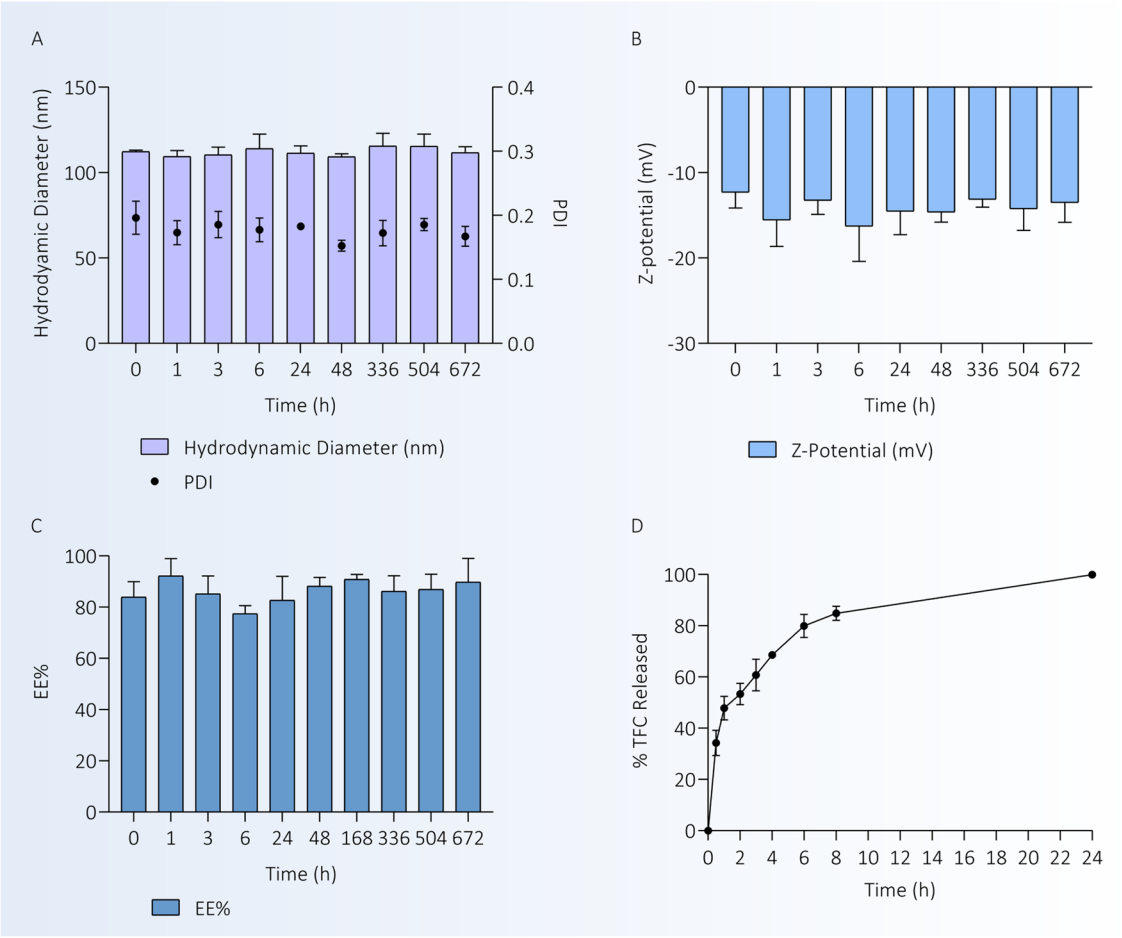

Figure 1. Stability over time in function of the physicochemical properties (hydrodynamic diameter and PDI (A), ζ-potential (B)) and of the encapsulation efficiency (EE) of TFC in the optimized formulation (C). Release curve of TFC in FaSSIF-V2 at pH 6.5 (D). Data are expressed as the mean ± standard deviation (n = 3).

each sample (NEs, and AGμ-NEs) was spread on the mucosal side and kept for 5 min for solution-mucosal interactions. The tissue was then washed with normal saline solution for 60 min (flow rate 6 mL/min, close system). The amount of tracer still on the tissue after 5, 10, 20, 30, 45, and 60 min of washing times was measured. Mucoadhesive capacity was calculated as the percentage of tracer retained by the mucosal tissue at the end of the process. The experiment was performed in triplicate. The assay of the tracer was performed using a fluorescence plate reader.

Statistical Analysis. For statistical analysis of the *ex vivo* and *in vitro* experiments, software GraphPad Prism 8.0 was used. Sidak's multiple-comparison test or two-tailed Student's *t*-test or the multiple *t*-test for unpaired samples were adopted, as specified for each experiment, and p values <0.05 were considered statistically significant. Data were expressed as the mean ± standard deviation of three independent experiments.

RESULTS

Nanoemulsion Preparation and Physicochemical Characterization. Stable NEs with a low polydispersity index (PDI) were obtained by the microfluidic technique. The optimization of the formulation considered the stability of the system in terms of the encapsulation efficiency, size, and surface charge, which are the parameters necessary for a stable and controlled drug release. The aqueous phase and the miscible organic solvent containing the precursors were separately injected into the microchannels under laminar flow, where the microscopic features engineered into the channel control the mixing of the two streams, leading to the production of homogeneous particles.[34] In the final suspen-

https://doi.org/10.1021/acs.biomac.3c00260
Biomacromolecules XXXX, XXX, XXX−XXX

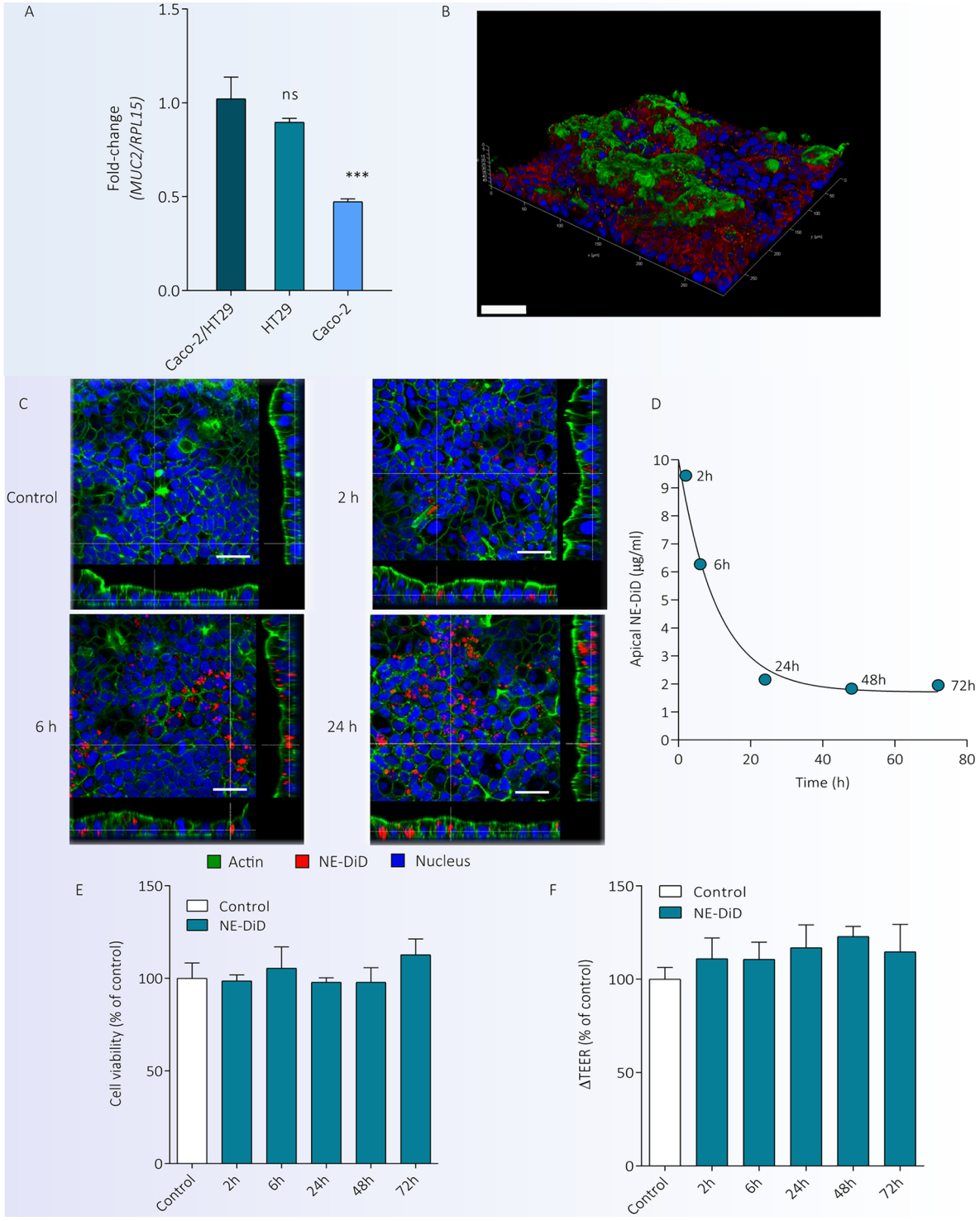

Figure 2. Relative gene expression of mucin-2 (*MUC2*) in Caco-2 and HT29-MTX, cultured alone or together (Caco-2/HT29-MTX). Data are normalized to the expression of the housekeeping gene *RPL15* and are expressed as folds of the mean value obtained in Caco-2/HT29-MTX monolayers kept at 1. ***$p < 0.001$ vs Caco-2/HT29-MTX, ns = not significant (*t*-test for unpaired samples) (A). A 3D reconstruction of a cell monolayer of Caco-2/HT29-MTX cells was obtained using the volume algorithm provided by LAS-X 4.5 software on Z-stack confocal images. Mucin-5 (MUC5AC) is in green, claudin-7 is in red, and nuclei are in blue. Bar = 50 μm (B). Caco-2/HT29-MTX monolayers were incubated in the presence of 1 μg/mL (C) or 10 μg/mL (D−F) of NE-DiD. Single horizontal confocal sections of representative fields of monolayers obtained after 2-, 6-, and 24 h of exposure are shown with orthogonal projections. Actin is rendered in green, NE-DiD in red, and nuclei in blue. In the control image, cells were cultured in the absence of NE-DiD. Bar = 50 μm (C). The concentration of NE-DiD in the apical medium after 2−6−24−48−72 h of incubation with Caco-2/HT29-MTX monolayers was measured and nonlinear regression analysis was used to obtain the curve (D). Cell viability (E) and TEER (F) of Caco-2/HT29-MTX monolayers are shown. Data are expressed as % of the control (cells cultured in the absence of NE-DiD). Data are the mean ± standard deviation of three independent experiments ($n = 3$).

https://doi.org/10.1021/acs.biomac.3c00260
Biomacromolecules XXXX, XXX, XXX−XXX

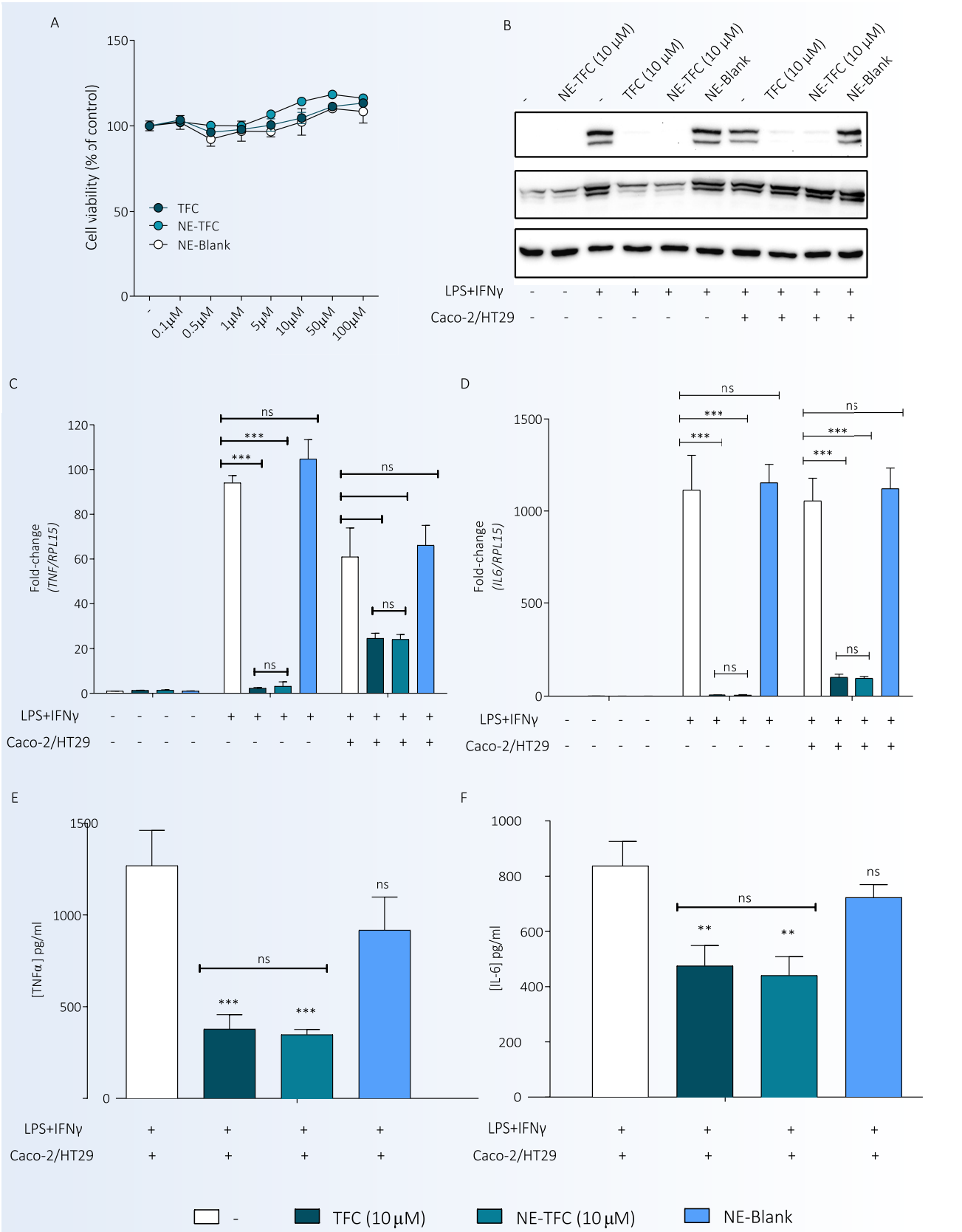

Figure 3. THP-1 cells were differentiated into macrophage-like cells, as described in Materials and Methods, and, after 48 h were incubated in the absence or in the presence of TFC, NE-TFC at increasing concentrations of the drug (0−100 μM) or NE-Blank. After a further 48 h, cell viability was evaluated (A). Data are expressed as % of the control (cells cultured in the absence of the drug or NEs). THP-1 macrophage-like cells were cultured for 24 h in monoculture or co-culture with Caco-2/HT29-MTX monolayers in the absence or in the presence of 10 μM TFC, NE-TFC, or of NE-Blank (90 μg/mL corresponding to the quantity of NE in the NE-TFC condition at 10 μM TFC), and of proinflammatory stimuli (LPS (100 ng/mL) and INF-γ (20 ng/mL)). A representative western blot of pSTAT1 and total STAT1 in THP-1 cells is shown in (B). Tubulin is used

https://doi.org/10.1021/acs.biomac.3c00260
Biomacromolecules XXXX, XXX, XXX−XXX

Figure 3. continued

for loading the control. Relative gene expression of *TNF* and *IL-6* in THP-1 cells is shown in (C) and (D), respectively. Data are normalized to the expression of the housekeeping gene *RPL15* and are expressed as folds of the mean value obtained in control cells (THP-1 cells cultured in monoculture in the absence of the drug or NEs) kept at 1. ***$p < 0.001$, ns = not significant (multiple *t*-test for unpaired samples). Secreted TNF-α and IL-6 into the medium by THP-1 cells were measured, and data are expressed as pg/mL, as shown in E and F, respectively. **$p < 0.01$, ***$p < 0.001$, ns = not significant vs control cells (THP-1 cells cultured in co-culture in the absence of the drug or NEs) (multiple *t*-test for unpaired samples). Data are the mean ± standard deviation of three independent experiments ($n = 3$).

sion, the lipid concentration was 14.3% w/v. To optimize the drug loading and to reduce the amount of formulation needed for the therapeutic activity, TFC was encapsulated into the nanosystem at three different concentrations. The maximum drug amount was chosen considering the solubility limit reached in the organic phase. All formulations (empty, drug-loaded, and DiD-loaded) presented a hydrodynamic diameter of around 111 nm, a slightly negative surface charge of around −15 mV derived from the PEGylated surfactant integrated into the particle shell, and a PDI lower than 0.2. NEs prepared at different drug concentrations resulted stable over 28 days in terms of physicochemical properties and the drug content, as shown in the Supporting information (Figure S1) and detailed in Table 1. No drug leakage was observed for the different systems at the storage conditions. The formulation that reached the maximal drug loading of 2.7% was chosen for the successive experiments (Figure 1A−C). The *in vitro* release of TFC from the NEs was evaluated under sink conditions in the intestinal fluid (FaSSIF-V2), as shown in Figure 1D. Almost half (48%) of the encapsulated TFC was released after 1 h of incubation in FaSSIF-V2 medium, 80% within 8 h, and a complete release was observed at 24 h.

***In Vitro* Internalization of Nanoemulsions into Mucus-Secreting Intestinal Cell Monolayers.** To study the biological impact of the nanoemulsions, we used a human mucus-secreting intestinal epithelial model[35] composed of two different cell types, HT29-MTX and Caco-2 cells, which reflect the key features of the human intestine epithelium. The first line synthesizes and secretes mucins, in particular, mucin-2 (*MUC2*, see the expression in Figure 2A) and mucin-5 (MUC5AC, see the tridimensional image in Figure 2B), whereas the latter expresses claudin-7 and shapes the tight junctions of the monolayer (Figure 2B). When the cell monolayer was exposed to NE-DiD, the red-stained fluorescence was increasingly visible in the cytosol of cells over the investigated time points (2-, 6-, 24 h, Figure 2C). The intracellular localization of DiD was evident in the orthogonal projections of the confocal images. Consistently, the concentration of the fluorescent signal in the apical compartment of the cell monolayer decreased over time compared to the initial time point (Figure 2D). The initial apical concentration was decreased by almost 40% after 6 h of exposure, dropped by more than 75% after 24 h, remaining nearly the same after 48 and 72 h, with a half-life of 7.3 h. Importantly, NEs did not alter either the viability (Figure 2E) or the TEER (Figure 2F) of the epithelial cell monolayer, even after long times of exposure. These results demonstrate that NEs are biocompatible and are internalized by human intestinal cell monolayers.

Anti-Inflammatory Activity of TFC-Loaded NEs on Macrophages in a Triple Cell Co-culture System. To evaluate if the encapsulated TFC exerts an anti-inflammatory activity on macrophages after internalization into the intestinal monolayer, we exploited a triple co-culture system where THP-1 macrophages, activated to a proinflammatory phenotype, were exposed to the drug through a monolayer of Caco-2/HT29-MTX cells, thus simulating the *in vivo* condition. TFC, NE-TFC, or empty NEs (NE-Blank) did not significantly modify cell viability in THP-1 macrophages maintained in monoculture (Figure 3A), confirming the biocompatibility of nanoemulsions. When THP-1 cells were activated with a proinflammatory stimulus (LPS + INFγ), they increased the expression of the phosphorylated fraction of STAT1, the target of JAK proteins (pSTAT1, Figure 3B). STAT1 activation was completely blocked by either TFC or NE-TFC at comparable levels, whereas it was not modified in the presence of NE-Blank. In co-culture with the Caco-2/HT29-MTX monolayer, activated THP-1 cells also increased pSTAT1 levels, which were almost totally suppressed by apical TFC or NE-TFC, although the total STAT1 protein level was highly increased. These results show that, since TFC encapsulated in NE inhibits the JAK-STAT pathway of macrophages at levels comparable to the free drug, NEs do not alter the anti-inflammatory activity of the drug. To confirm this result, we measured gene expression (Figure 3C,D) and the secreted fraction (Figure 3E,F) of the inflammatory cytokines TNF-α and IL-6 in THP-1 cells stimulated with LPS+INFγ in the absence or in the presence of TFC or NE-TFC. As expected, stimulated THP-1 cells markedly increased the expression of the two cytokines in either monoculture or co-culture with Caco-2/HT29-MTX monolayers. In the presence of TFC or NE-TFC, the induction of *TNF* and *IL-6* was completely hindered when THP-1 cells were in direct contact with the drug (monoculture) and significantly lowered in the co-culture system (Figure 3C,D), where the fraction of secreted TNF-α and IL-6 was reduced by more than 65 and 40%, respectively, in the presence of either TFC or NE-TFC (Figure 3E,F).

AGμ and AGμ-NE Morphological and Rheological Characterizations. To increase the residence time of the NEs in the gastrointestinal tract, AG was selected as a biopolymer for the formulation of a bio- and mucoadhesive hybrid nanocomposite. AGμ was produced by the ionotropic gelation technique using a Microencapsulator B-395 apparatus equipped with a single nozzle system. At first, empty microbeads were prepared and analyzed by optical microscopy (Leica DM1000 microscope, 5× magnification). Images revealed the regular and spherical shape of alginate microbeads with the absence of any aggregation (Figure 4A). NE-TFC (5% w/v) were embedded into the alginate structure in order to obtain nanocomposites AGμ-NE. Optical microscopy images showed the encapsulation of NEs into alginate microbeads, which caused the presence of a homogeneous opacity within the beads' outline (Figure 4B). The diameter of at least 30 microbeads was measured in triplicate using ImageJ software to calculate the mean diameter (Figure 4C). AGμ with an average diameter of 262 ± 22 μm was obtained using a 200 μm single nozzle. A slight increase in the average diameter was observed

https://doi.org/10.1021/acs.biomac.3c00260
Biomacromolecules XXXX, XXX, XXX−XXX

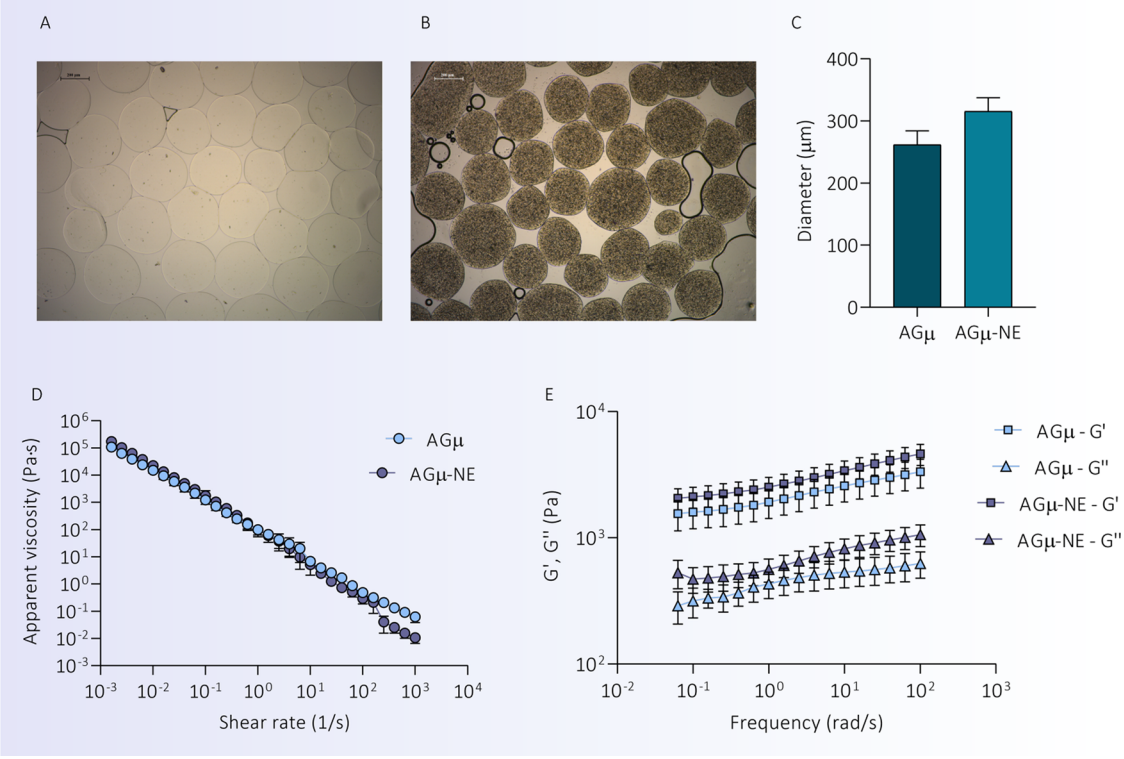

Figure 4. Optical microscopy images of empty AGμ (A) and nanocomposites AGμ-NE (B), and the average diameter measured with ImageJ software (C). Flow sweep tests of AGμ (light blue dots) and AGμ-NE (purple dots) expressed in terms of the apparent viscosity (D). Frequency sweep tests of AGμ and AGμ-NE before drying (E) expressed in terms of apparent G' and G'' moduli. Data are expressed as the mean ± standard deviation (n = 3).

in AGμ-NE compared to the empty ones, with an average diameter of 315 ± 22 μm.

The flow behavior and the viscoelastic properties of AGμ and AGμ-NE were assessed through rheological analyses. Flow sweep tests were performed on the samples directly after their preparation. The apparent viscosity (η) of samples was measured at a shear rate ($\dot{\gamma}$) range of 0.001−1000 s^{-1} and at a temperature of 24 °C. The samples are suspensions constituted by a continuous phase (aqueous) and microgel particles. The flow behavior of the relatively concentrated microgel suspension is intimately related to the movements of the particles. Results showed a decrease in the apparent viscosity as the shear rate increased for all of the tested samples (Figure 4D). This trend confirms a shear-thinning behavior for the AG microbead suspension due to the shear-induced breaking of interparticle linkages at high shear rates, a behavior typically observed in microgel suspensions.[36,37] No significant difference was observed between AGμ and AGμ-NE in terms of the apparent viscosity, meaning that the incorporation of NEs did not modify the overall flow behavior of the suspension. Then, dynamic rheological characterizations were performed. Strain sweep tests (data not shown) allowed us to identify the LVE region and fix a strain of 0.3% for frequency sweep tests. Beyond the LVE region, a further increase in strain resulted in a decrease of the apparent rheological G' and G'' moduli, meaning that the structure of AG microbeads broke down. Frequency sweep measurements (Figure 4E) were performed directly after sample preparation within the LVE region in the range of 100−0.05 rad/s to measure the apparent storage modulus G' and the apparent loss modulus G″. G' represents the elastic component of the material behavior, whereas G″ represents the viscous component. All of the samples presented the same trend: G' was higher than G″ in the frequency range measured, and the loss tangent (equal to G″/G') was lower than 1 for all of the samples, conditions that define a solid-like rheological behavior and that are representative of highly structured samples. Moreover, the apparent G' and G'' moduli slightly increased with frequency. This frequency dependence is typically observed for soft matter systems and microgel suspensions.[38] Lastly, G' and G'' result slightly higher in the presence of NE than in their absence, and the suspension appears to behave more solid-like.

Stability of Freeze-Dried AGμ and AGμ-NE, *In Vitro* Drug Release and Structural Characterization in Biorelevant Fluids. Microbeads were freeze-dried to enable their long-term storage. White powders with good flowability and the absence of stickiness were obtained for both AGμ and AGμ-NE. The morphology of lyophilized AGμ and AGμ-NE was analyzed by SEM. The images in Figure 5A,B reveal the loss of the microbeads' spherical shape due to the collapsing of the structure caused by the removal of water after drying. The residual water content was investigated by TGA, and it was about 15% in the raw powders. AGμ showed a lower residual moisture content than corresponding powders, which was in the same range (6−7%) when compared to AGμ-NE, with or without the loaded drug. These differences in residual water contents show that AGμ and AGμ-NE are slightly less hydrophilic than alginate powders, due to the presence of hydrophobic interactions between the AG chains in the AGμ and AGμ-NE and to the presence of lipids in the AGμ-NE formulation. Results are summarized in Figure 5C. The loading capacity (LC%) of TFC obtained using eq 5 was 3.75 ± 0.14%.

https://doi.org/10.1021/acs.biomac.3c00260
Biomacromolecules XXXX, XXX, XXX−XXX

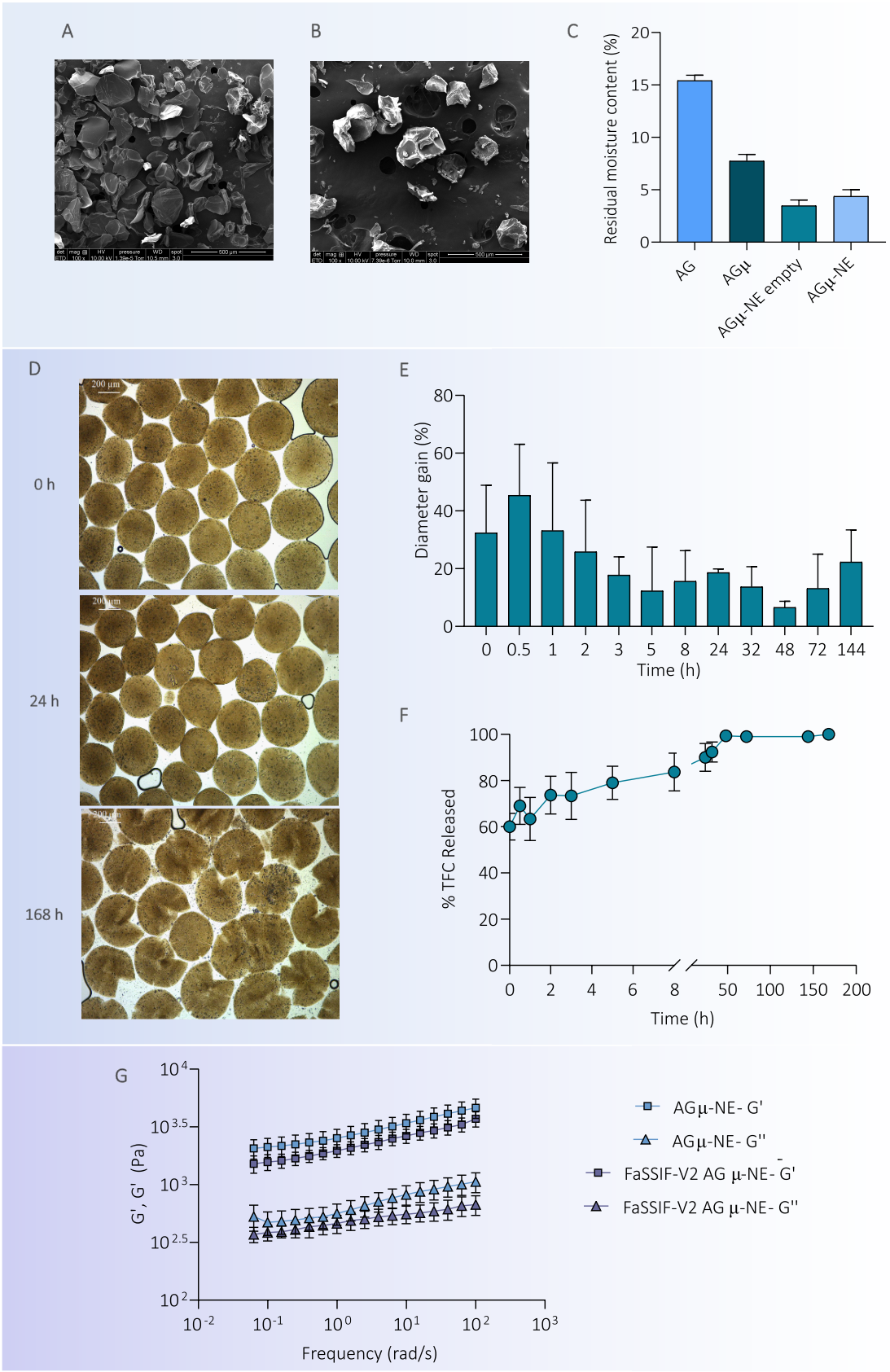

Figure 5. SEM images of AGμ (A) and nanocomposites AGμ-NE (B) post freeze-drying. Residual moisture content detected in the different samples by TGA (C). 5X magnification optical microscopy pictures of AGμ FaSSIF-V2 (pH 6.5) at different time points of the stability study (D). Diameter gain AGμ in FaSSIF-V2 (pH 6.5) buffer (E). Time course of the TFC *in vitro* release profile in collected FaSSIF-V2 (pH 6.5) buffer (F). Comparison of frequency sweep tests of AGμ-NE before drying and after rehydration in FaSSIF-V2 (G) expressed in terms of apparent G' and G'' moduli. Data are expressed as the mean ± standard deviation (n = 3).

https://doi.org/10.1021/acs.biomac.3c00260
Biomacromolecules XXXX, XXX, XXX−XXX

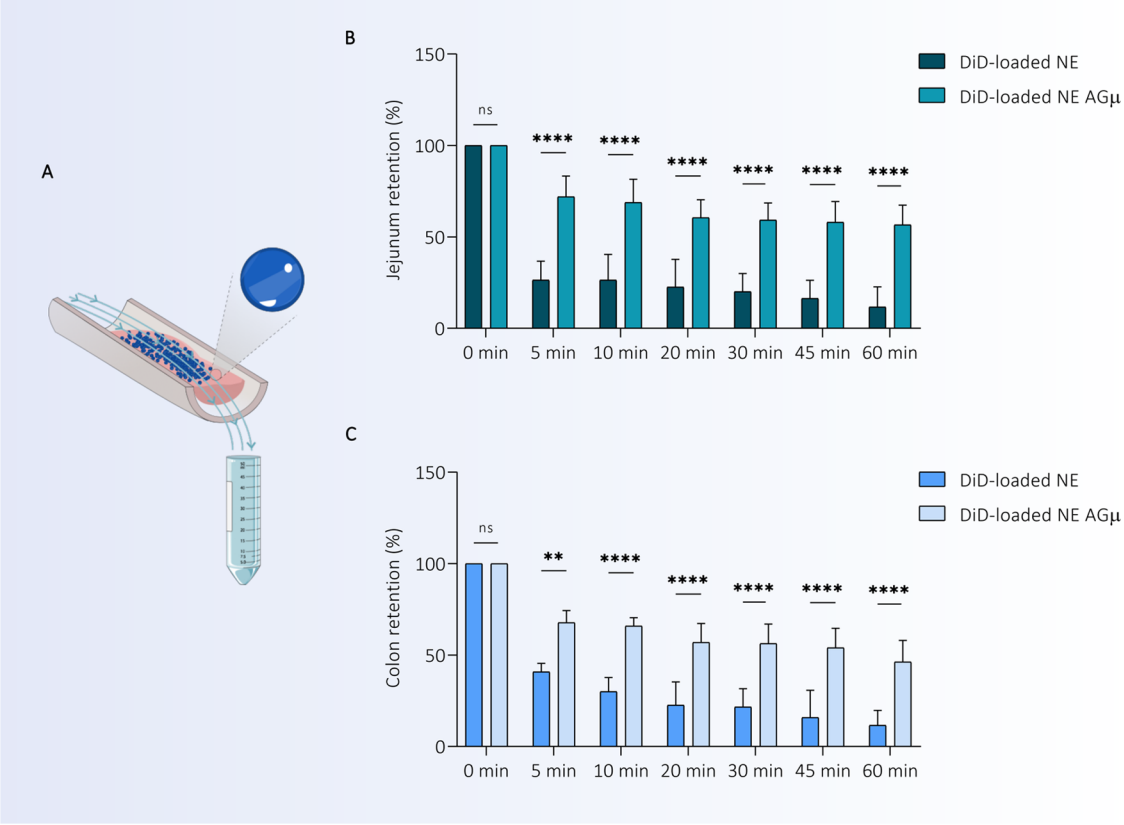

Figure 6. Schematic representation of the mucoadhesion study setup. (A). Percentage of retention on the rat jejunum (B) and colon (C) mucosa over a period of 60 min. Data are shown as the mean ± standard deviation (n = 3). Statistical data analysis on Sidak's multiple comparison test: *p < 0.05; **p < 0.01; ***p < 0.001; ****p < 0.0001; ns = not significant.

AGμ and AGμ-NE were rehydrated in simulated intestinal fluids (FaSSIF-V2) containing physiological concentrations of calcium, which plays a key role in the alginate hydrogel formation. Physiological levels of calcium enhance the stability of AG microbeads preventing degradation and loss of their structural integrity, limiting the ion exchange process between monovalent ions in GI fluids and Ca^{2+} ions in the cross-linked AG microbeads.[39] To assess their stability, resuspended empty microbeads were analyzed by optical microscopy to detect structural changes over a period of 7 days. The mean diameter of microbeads was measured on optical microscopy images using ImageJ software (see the Supporting information, Figure S2). At the first time point (0 h), images shown in Figure 5D revealed the successful rehydration of the microbeads and the complete recovery of the spherical shape. The microbeads reached an average diameter of 446 ± 82 μm, and a loss of the round shape with defined edges was observed at 168 h, a sign of degradation of the hybrid system. The time-dependent size variations showing an increasing over time (Figure 5E) were assessed by calculating the diameter gain (eq 6) compared to the size of microbeads before drying. The release of TFC-loaded NEs from AGμ-NE was evaluated *in vitro* in simulated intestinal fluids over a period of 7 days. At each of the defined time points, FaSSIF-V2 supernatants were analyzed by DLS in order to confirm the release of the whole NE (data not shown), proving the presence of the nanosystem in the medium. For each time point, TFC present in the supernatant was quantified by RP-HPLC analyses. Results were normalized according to the total TFC embedded in microbeads measured as the maximum released amount reached after 7 days. As shown in Figure 5F, in FaSSIF-V2 at pH 6.5, an immediate burst release of 60% of the drug was observed upon rehydration, followed by a slower phase reaching 80% of the release in 5 h, to end with a total drug release 60 h after bead resuspension.

Frequency sweep tests were repeated on dried AGμ-NE 12 hours after the resuspension in FaSSIF-V2 in order to verify the impact of the complex medium on the sample viscoelastic properties. Results showed the same trend of apparent G' and G'' moduli depending on the frequency as reported for AG microbeads before drying, confirming the behavior of soft gels (Figure 5G). Values of apparent G' and G'' were slightly higher when microbeads were loaded with NE. In general, no significant difference was observed between the empty and the NE-loaded beads.

Mucoadhesive Properties of AGμ-NE on the Intestinal Mucosa of Rats. The percentage of AG microbeads retained on rat intestines (jejunum and colon) over a period of 60 min was used to evaluate the mucoadhesive properties of microbeads. AGμ-NE were formulated with DiD-loaded NEs. The nanocomposites exhibited good mucoadhesive properties with significant differences when compared with DiD-loaded NEs alone, which were rapidly washed out (Figure 6). Furthermore, no specificity for either intestinal tract was demonstrated by these studies. NEs showed a retention ability of around 30%, while the nanocomposites displayed an increased adhesion ability with a 60−70% of retention on the rat intestinal mucosa.

https://doi.org/10.1021/acs.biomac.3c00260
Biomacromolecules XXXX, XXX, XXX−XXX

DISCUSSION

Drug delivery systems, and especially lipid-based nanosystems, have received a great deal of attention, thanks to their ability to overcome the biological barriers upon oral administration.[40] Lipids and lipophilic excipients can have significant and beneficial effects on the oral delivery of hydrophobic drugs.[41] However, the *in vitro* and especially the *in vivo* performances of these lipid systems are poorly predictable, limiting their use for enhancing drug exposure. These considerations underlie the rationale behind the creation of lipid−polymer hybrid nanocomposites, as a strategy to control the *in vivo* behavior of nanosystems and to limit their intrinsic variability upon oral administration.[7]

NEs have been widely explored as delivery systems for oral administration, allowing high entrapment efficiency of hydrophobic drugs. NEs are often manufactured, implying lengthy and noncontinuous strategies, which are responsible for high degrees of batch-to-batch variability, limiting industrial development.[42] To address this challenge, microfluidic technologies have been used to synthesize lipid-based NPs with more controlled physical properties, improving process accuracy and efficiency and also in the sight of possible up-scaling.[43] Although the advantages of microfluidics in preparing lipid systems are known, only a few adopted this technology for the formulation of NEs,[44] and the drug-loaded systems are still often prepared using conventional techniques.[45] Here, we proved the feasibility of a technology transfer in the preparation of drug-loaded NEs, maintaining the physicochemical parameters of the original formulation,[24] but with significant improvement in the reproducibility and scalability of the final suspension. In fact, the prepared NE meets all of the requirements related to physicochemical properties as well as long-term stability, thus supporting the potential use of this system for drug delivery (Figure 1 A, B, and C). The microfluidic approach adopted here also allowed the loading of a considerably higher amount of TFC in the NEs when compared to classical methods, which can be translated into an improved tolerability *in vivo*.

To evaluate the biological effects of the NE-TFC and simulate their behavior when in contact with an inflamed intestinal epithelium, NEs were tested on co-cultures of human intestinal epithelial monolayers and macrophages. At variance with a previous study, in which TFC activity was evaluated in a co-culture of THP-1 macrophages and a monolayer formed by Caco-2 cells only,[46] we have adopted here a triple co-culture, where the intestinal cell monolayer is composed of two cell populations, Caco-2 and mucus-secreting HT29-MTX cells. Thus, this intestinal monolayer is characterized by the simultaneous presence of tight junctions and mucus on the surface in order to mimic as far as possible the *in vivo* conditions.[31,35] NEs were quickly internalized by the mucus-secreting intestinal cell monolayer (half time about 7 h) and were clearly detected in the cytosol (Figure 2C−D), suggesting that NEs favor bioavailability in the bowel epithelium. Moreover, the TFC loaded into NEs, internalized by the cell monolayer, clearly inhibited the activation of the JAK-STAT pathway in subepithelial macrophages stimulated by a proinflammatory stimulus, a condition that mimics IBD. Consistently, NE-TFC hindered the synthesis and secretion of the proinflammatory cytokines TNF-α and IL-6 (Figure 3). These results confirmed that the proposed lipid nanosystem efficiently delivers TFC without altering the anti-inflammatory properties of the drug.

To overcome the problem of poor bioadhesion of the nanosystems, we selected AG as biopolymers for the development of hybrid nanocomposites aiming at prolonging NE retention time in the intestinal tract, thus improving drug availability. AG microbeads with a diameter of around 300 μm and a spherical shape were obtained by optimizing the formulation parameters. As previously reported,[11] the method adopted allowed the preparation of beads with a homogeneous dispersion of NEs within the beads' outline (Figure 4B). In bulk polysaccharide hydrogels, composite gel behavior can be influenced by the interaction between the gel matrix and the embedded nanoparticles.[47] Even if gel microbeads and bulk hydrogels share important similarities in their architecture, their rheological behaviors are significantly different. The microbead-based system is a macroscopic suspension constituted by a continuous phase (water) and gel microparticles.[36] The study of the apparent viscosity of the suspensions (Figure 4D) performed on both AGμ and AGμ-NE revealed a shear-thinning behavior for all samples, typically observed in microgel suspensions.[37] The apparent viscosity decreases as the shear rate increases. The structural events, such as the breaking of interparticle bridges, during the rheological measurements, are responsible for the shear-thinning behavior. Finally, the incorporation of NE in AG microbeads did not modify the overall flow behavior of the suspensions, and no significant differences were observed between AGμ and AGμ-NE. Additionally, a solid-like rheological behavior of both microbeads (with and without NE) was observed by dynamic rheological characterizations applying frequency sweep tests. More precisely, the resulting curves of the rheological moduli are typical of soft matter systems and microgel suspensions, showing a small increase of the apparent moduli with the frequency. A slight rise in the apparent moduli was observed for AGμ-NE, suggesting that the nanosystems entangled in the hydrogel structure produce slightly stiffer systems and that the presence of interactions between NE and AG strengthen the composite.

To guarantee long-term storage of the final system, AGμ and AGμ-NE were successfully freeze-dried without affecting TFC loading. Moreover, the encapsulation of NE into AG microbeads confirmed the advantage of nanocomposites in enhancing the final drug loading by 38.9%, from 2.7 to 3.75%. As highlighted by the SEM images (Figure 5A,B), the loss of water content led to the complete shrinking of the beads, possibly causing a partial expulsion of the lipid particles, which may be placed on the lyophilized surface. In fact, in terms of weight, the quantity of lipids is 5-fold higher than that of the polysaccharide. To get insights into the stability of the formulations in the intestinal tract, the nanocomposites were exposed to simulated intestinal fluids (FaSSIF-V2) (Figure 5D−F). A complete recovery of the spherical shape of dried microbeads was obtained after resuspension in FaSSIF-V2. Diameter gain data (Figure 5E) revealed the trend of AG microbeads to swell in intestinal-like conditions due to AG pH-dependent behavior, in accordance with what was recently highlighted by Gomez et al.[16] Indeed, at intestinal pH values, swelling occurs, thanks to the increased repulsive charges between AG chains due to deprotonated negatively charged carboxylic acid groups. The images in Figure 5D show the beginning of the disintegration of the microbeads starting from 168 h (1 week) after the resuspension, probably due to the fact

https://doi.org/10.1021/acs.biomac.3c00260
Biomacromolecules XXXX, XXX, XXX−XXX

that ionically cross-linked alginate hydrogels can dissolve by exchanging Ca^{2+} with Na^{+} ions.[48] The *in vitro* release profile of TFC from resuspended nanocomposites was then studied (Figure 5F). An immediate release of 60% of the drug was observed, probably as a consequence of the freeze-drying process in which the AG-based microbeads lose around 95% of their volume. To overcome these hurdles, several strategies can be easily explored, such as the use of pH-dependent polymers as the coating of the microgel, such as Eudragit polymers, RPLO, and S100.[49] For example, Giri et al. encapsulated drug-loaded liposomes in alginate hydrogel beads, followed by coating with Eudragit S-100 for efficient colonic delivery.[50]

Nevertheless, we have proved by *ex vivo* studies on the rat jejunum and colon mucosa that assisted site-specific targeting can be promoted by AG mucoadhesive properties. Indeed, the results shown in Figure 6 confirmed the ability of AGμ to be retained on the intestinal mucosa, thus favoring local drug delivery. Mucoadhesive properties of microparticles based on polysaccharides were similarly investigated by Duan et al. on inflamed colon mucosa, confirming the advantage of specific drug delivery to the site of inflammation, thanks to the bioadhesive characteristics conferred to the drug delivery system.[13]

CONCLUSIONS

By combining nanoemulsions and an alginate-based hydrogel matrix, we have created a hybrid nanocomposite as a platform for the localized delivery of lipophilic compounds by oral administration. A microfluidic approach for an optimized formulation of NEs was set up, maximizing tofacitinib loading and the stability of the system. A triple cell culture model, mimicking the inflammatory conditions at the intestinal level, proved the ability of the NEs to penetrate the mucus covering the epithelium and to mediate the internalization of the drug, which can pass intact through the underlying epithelium and exert its anti-inflammatory activity on activated macrophages. Alginate microbeads, exploited as matrices to enhance the performance of the orally administered nanosystem, were successfully prepared and dried for long-term stability. A high bioadhesion at the level of both intestinal and colonic mucosa was proven by *ex vivo* studies on excised segments of the rat small intestine and colon. Altogether, these results support the use of the novel hybrid nanosystem described here to deliver anti-inflammatory drugs to the intestine. Moreover, this approach is a potentially transposable platform for the localized oral administration of a variety of small molecules.

ASSOCIATED CONTENT

Supporting Information

The Supporting Information is available free of charge at https://pubs.acs.org/doi/10.1021/acs.biomac.3c00260.

> Primers used to evaluate gene expression; stability over time in function of the physicochemical properties (hydrodynamic diameter and PdI, ζ-potential), and of the encapsulation efficiency of TFC of the formulation prepared at a final drug concentration of 2 or 4 mg/mL; and stability of the mean diameter of NE-TFC-loaded AG microbeads resuspended in FaSSIF-V2 (pH 6.5) (PDF)

AUTHOR INFORMATION

Corresponding Author

Giovanna Lollo − *Univ Lyon, Université Claude Bernard Lyon 1, CNRS, LAGEPP UMR 5007, F-69622 Villeurbanne, France;* orcid.org/0000-0001-7030-3056; Email: giovanna.lollo@univ-lyon1.fr

Authors

Valentina Andretto − *Univ Lyon, Université Claude Bernard Lyon 1, CNRS, LAGEPP UMR 5007, F-69622 Villeurbanne, France*

Giuseppe Taurino − *Laboratory of General Pathology, Department of Medicine and Surgery, University of Parma, 43125 Parma, Italy; MRH-Microbiome Research Hub, Parco Area delle Scienze 11/A, University of Parma, 43124 Parma, Italy;* orcid.org/0000-0001-9606-1171

Giulia Guerriero − *Univ Lyon, Université Claude Bernard Lyon 1, CNRS, LAGEPP UMR 5007, F-69622 Villeurbanne, France*

Hanäé Guérin − *Univ Lyon, Université Claude Bernard Lyon 1, CNRS, LAGEPP UMR 5007, F-69622 Villeurbanne, France*

Emmanuelle Lainé − *Université Clermont Auvergne, INRAe, UMR454 MEDIS (Microbiologie, Environnement Digestif et Santé), 63000 Clermont-Ferrand, France*

Massimiliano G. Bianchi − *Laboratory of General Pathology, Department of Medicine and Surgery, University of Parma, 43125 Parma, Italy; MRH-Microbiome Research Hub, Parco Area delle Scienze 11/A, University of Parma, 43124 Parma, Italy*

Géraldine Agusti − *Univ Lyon, Université Claude Bernard Lyon 1, CNRS, LAGEPP UMR 5007, F-69622 Villeurbanne, France*

Stéphanie Briançon − *Univ Lyon, Université Claude Bernard Lyon 1, CNRS, LAGEPP UMR 5007, F-69622 Villeurbanne, France*

Ovidio Bussolati − *Laboratory of General Pathology, Department of Medicine and Surgery, University of Parma, 43125 Parma, Italy; MRH-Microbiome Research Hub, Parco Area delle Scienze 11/A, University of Parma, 43124 Parma, Italy*

Alexandra Clayer-Montembault − *Univ Lyon, Université Claude Bernard Lyon 1, INSA Lyon, Université Jean Monnet, CNRS, UMR 5223, Ingénierie des Matériaux Polymères (IMP), F-69622 Villeurbanne, France*

Complete contact information is available at: https://pubs.acs.org/10.1021/acs.biomac.3c00260

Author Contributions

#V.A. and G.T. contributed equally.

Notes

The authors declare no competing financial interest.

ACKNOWLEDGMENTS

The HyDNano project (ANR-18-CE18-0025-01), Valentina Andretto fellowship was funded by the National Research Agency (ANR). Giuseppe Taurino was supported by a research fellowship of the Microbiome Research Hub of the University of Parma funded by Fondazione Cariparma. The confocal experiments were carried out at the Confocal Microscopy Lab. (Dept. of Medicine and Surgery, University of Parma), and the cost of the Leica STELLARIS 5 confocal

system was partly supported by the University of Parma through the Scientific Instrumentation Upgrade Program 2019.

REFERENCES

(1) Matha, K.; Lollo, G.; Taurino, G.; Respaud, R.; Marigo, I.; Shariati, M.; Bussolati, O.; Vermeulen, A.; Remaut, K.; Benoit, J. P. Bioinspired Hyaluronic Acid and Polyarginine Nanoparticles for DACHPt Delivery. *Eur. J. Pharm. Biopharm.* **2020**, *150*, 1−13.

(2) Repellin, M.; Carton, F.; Boschi, F.; Galiè, M.; Perduca, M.; Calderan, L.; Jacquier, A.; Carras, J.; Schaeffer, L.; Briançon, S.; Lollo, G.; Malatesta, M. Repurposing Pentamidine Using Hyaluronic Acid-Based Nanocarriers for Skeletal Muscle Treatment in Myotonic Dystrophy. *Nanomedicine* **2023**, *47*, No. 102623.

(3) Rosso, A.; Almouazen, E.; Pontes, J.; Andretto, V.; Leroux, M.; Romasko, E.; Azzouz-Maache, S.; Bordes, C.; Coste, I.; Renno, T.; Giraud, S.; Briancon, S.; Lollo, G. Supersaturable Self-Microemulsifying Delivery Systems: An Approach to Enhance Oral Bioavailability of Benzimidazole Anticancer Drugs. *Drug Delivery Transl. Res.* **2021**, *11*, 675−691.

(4) Shi, Y.; Lammers, T. Combining Nanomedicine and Immunotherapy. *Acc. Chem. Res.* **2019**, *52*, 1543−1554.

(5) Zhang, C.; Yan, L.; Wang, X.; Zhu, S.; Chen, C.; Gu, Z.; Zhao, Y. Progress, Challenges, and Future of Nanomedicine. *Nano Today* **2020**, *35*, No. 101008.

(6) Andretto, V.; Rosso, A.; Briançon, S.; Lollo, G. Nanocomposite Systems for Precise Oral Delivery of Drugs and Biologics. *Drug Delivery Transl. Res.* **2021**, *11*, 445−470.

(7) Desfrançois, C.; Auzély, R.; Texier, I. Lipid Nanoparticles and Their Hydrogel Composites for Drug Delivery: A Review. *Pharmaceuticals* **2018**, *11*, 118.

(8) Merino, S.; Martín, C.; Kostarelos, K.; Prato, M.; Vázquez, E. Nanocomposite Hydrogels: 3D Polymer−Nanoparticle Synergies for On-Demand Drug Delivery. *ACS Nano* **2015**, *9*, 4686−4697.

(9) Abdellatif, A. A. H.; Ibrahim, M. A.; Amin, M. A.; Maswadeh, H.; Alwehaibi, M. N.; Al-Harbi, S. N.; Alharbi, Z. A.; Mohammed, H. A.; Mehany, A. B. M.; Saleem, I. Cetuximab Conjugated with Octreotide and Entrapped Calcium Alginate-Beads for Targeting Somatostatin Receptors. *Sci. Rep.* **2020**, *10*, No. 4736.

(10) Sun, R.; Xia, Q. Nanostructured Lipid Carriers Incorporated in Alginate Hydrogel: Enhanced Stability and Modified Behavior in Gastrointestinal Tract. *Colloids Surf., A* **2019**, *574*, 197−206.

(11) Taipaleenmäki, E.; Christensen, G.; Brodszkij, E.; Mouritzen, S. A.; Gal, N.; Madsen, S.; Hedemann, M. S.; Knudsen, T. A.; Jensen, H. M.; Christiansen, S. L.; Sparsø, F. V.; Städler, B. Mucopenetrating Polymer − Lipid Hybrid Nanovesicles as Subunits in Alginate Beads as an Oral Formulation. *J. Controlled Release* **2020**, *322*, 470−485.

(12) Iglesias, N.; Galbis, E.; Díaz-Blanco, M. J.; Lucas, R.; Benito, E.; De-Paz, M. V. Nanostructured Chitosan-Based Biomaterials for Sustained and Colon-Specific Resveratrol Release. *Int. J. Mol. Sci.* **2019**, *20*, 398.

(13) Duan, B.; Li, M.; Sun, Y.; Zou, S.; Xu, X. Orally Delivered Antisense Oligodeoxyribonucleotides of TNF-α via Polysaccharide-Based Nanocomposites Targeting Intestinal Inflammation. *Adv. Healthcare Mater.* **2019**, *8*, No. 1801389.

(14) Khare, T.; Palakurthi, S. S.; Shah, B. M.; Palakurthi, S.; Khare, S. Natural Product-Based Nanomedicine in Treatment of Inflammatory Bowel Disease. *Int. J. Mol. Sci.* **2020**, *21*, 3956.

(15) Agüero, L.; Zaldivar-Silva, D.; Peña, L.; Dias, M. L. Alginate Microparticles as Oral Colon Drug Delivery Device: A Review. *Carbohydr. Polym.* **2017**, *168*, 32−43.

(16) Gómez-Mascaraque, L. G.; Martínez-Sanz, M.; Hogan, S. A.; López-Rubio, A.; Brodkorb, A. Nano- and Microstructural Evolution of Alginate Beads in Simulated Gastrointestinal Fluids. Impact of M/G Ratio, Molecular Weight and PH. *Carbohydr. Polym.* **2019**, *223*, No. 115121.

(17) Abdellatif, A. A. H.; El Hamd, M. A.; Saleh, k. i. A Formulation, Optimization and Evaluation of Controlled Released Alginate Beads Loaded-Flurbiprofen. *J. Nanomed. Nanotechnol.* **2016**, *07*, 357.

(18) Ferreira, N. N.; Caetano, B. L.; Boni, F. I.; Sousa, F.; Magnani, M.; Sarmento, B.; Ferreira Cury, B. S.; Daflon Gremião, M. P. Alginate-Based Delivery Systems for Bevacizumab Local Therapy: In Vitro Structural Features and Release Properties. *J. Pharm. Sci.* **2019**, *108*, 1559−1568.

(19) Senna, J. P.; Barradas, T. N.; Cardoso, S.; Castiglione, T. C.; Serpe, M. J.; de Holanda e Silva, K. G.; Mansur, C. R. E. Dual Alginate-Lipid Nanocarriers as Oral Delivery Systems for Amphotericin B. *Colloids Surf., B* **2018**, *166*, 187−194.

(20) Li, W.; Li, Y.; Liu, Z.; Kerdsakundee, N.; Zhang, M.; Zhang, F.; Liu, X.; Bauleth-Ramos, T.; Lian, W.; Mäkilä, E.; Kemell, M.; Ding, Y.; Sarmento, B.; Wiwattanapatapee, R.; Salonen, J.; Zhang, H.; Hirvonen, J. T.; Liu, D.; Deng, X.; Santos, H. A. Hierarchical Structured and Programmed Vehicles Deliver Drugs Locally to Inflamed Sites of Intestine. *Biomaterials* **2018**, *185*, 322−332.

(21) Zhang, S.; Langer, R.; Traverso, G. Nanoparticulate Drug Delivery Systems Targeting Inflammation for Treatment of Inflammatory Bowel Disease. *Nano Today* **2017**, *16*, 82−96.

(22) Sosnik, A. Alginate Particles as Platform for Drug Delivery by the Oral Route: State-of-the-Art. *ISRN Pharm.* **2014**, *2014*, 1−17.

(23) Rosso, A.; Andretto, V.; Chevalier, Y.; Kryza, D.; Sidi-Boumedine, J.; Grenha, A.; Guerreiro, F.; Gharsallaoui, A.; La Padula, V.; Montembault, A.; David, L.; Briançon, S.; Lollo, G. Nanocomposite Sponges for Enhancing Intestinal Residence Time Following Oral Administration. *J. Controlled Release* **2021**, *333*, 579−592.

(24) Amante, C.; Andretto, V.; Rosso, A.; Augusti, G.; Marzocco, S.; Lollo, G.; Del Gaudio, P. Alginate-Pectin Microparticles Loaded with Nanoemulsions as Nanocomposites for Wound Healing. *Drug Delivery Transl. Res.* **2023**, *13*, 1343−1357.

(25) Sandborn, W. J.; Su, C.; Sands, B. E.; D'Haens, G. R.; Vermeire, S.; Schreiber, S.; Danese, S.; Feagan, B. G.; Reinisch, W.; Niezychowski, W.; Friedman, G.; Lawendy, N.; Yu, D.; Woodworth, D.; Mukherjee, A.; Zhang, H.; Healey, P.; Panés, J. Tofacitinib as Induction and Maintenance Therapy for Ulcerative Colitis. *N. Engl. J. Med.* **2017**, *376*, 1723−1736.

(26) Panés, J.; Sandborn, W. J.; Schreiber, S.; Sands, B. E.; Vermeire, S.; D'Haens, G.; Panaccione, R.; Higgins, P. D. R.; Colombel, J. F.; Feagan, B. G.; Chan, G.; Moscariello, M.; Wang, W.; Niezychowski, W.; Marren, A.; Healey, P.; Maller, E. Tofacitinib for Induction and Maintenance Therapy of Crohn's Disease: Results of Two Phase IIb Randomised Placebo-Controlled Trials. *Gut* **2017**, *66*, 1049−1059.

(27) Hodge, J. A.; Kawabata, T. T.; Krishnaswami, S.; Clark, J. D.; Telliez, J.-B.; Dowty, M. E.; Menon, S.; Lamba, M.; Zwillich, S. The Mechanism of Action of Tofacitinib - an Oral Janus Kinase Inhibitor for the Treatment of Rheumatoid Arthritis. *Clin. Exp. Rheumatol.* **2016**, *34*, 318−328.

(28) Choy, E. H. Clinical Significance of Janus Kinase Inhibitor Selectivity. *Rheumatology* **2019**, *58*, 953−962.

(29) De Vries, L. C. S.; Wildenberg, M. E.; De Jonge, W. J.; D'Haens, G. R. The Future of Janus Kinase Inhibitors in Inflammatory Bowel Disease. *J. Crohn's Colitis* **2017**, *11*, 885−893.

(30) Feagan, B. Update on Tofacitinib for Inflammatory Bowel Disease. *Gastroenterol. Hepatol.* **2016**, *12*, 572−574.

(31) Li, Y.; Arranz, E.; Guri, A.; Corredig, M. Mucus Interactions with Liposomes Encapsulating Bioactives: Interfacial Tensiometry and Cellular Uptake on Caco-2 and Cocultures of Caco-2/HT29-MTX. *Food Res. Int.* **2017**, *92*, 128−137.

(32) Bustin, S. Absolute Quantification of MRNA Using Real-Time Reverse Transcription Polymerase Chain Reaction Assays. *J. Mol. Endocrinol.* **2000**, *25*, 169−193.

(33) Cook, M. T.; Khutoryanskiy, V. V. Mucoadhesion and Mucosa-Mimetic Materials-A Mini-Review. *Int. J. Pharm.* **2015**, *495*, 991−998.

(34) Streck, S.; Hong, L.; Boyd, B. J.; McDowell, A. Microfluidics for the Production of Nanomedicines: Considerations for Polymer and Lipid-Based Systems. *Pharm. Nanotechnol.* **2019**, *7*, 423−443.

(35) Bianchi, M. G.; Chiu, M.; Taurino, G.; Brighenti, F.; Del Rio, D.; Mena, P.; Bussolati, O. Catechin and Procyanidin B2 Modulate the Expression of Tight Junction Proteins but Do Not Protect from

https://doi.org/10.1021/acs.biomac.3c00260
Biomacromolecules XXXX, XXX, XXX−XXX

Inflammation-Induced Changes in Permeability in Human Intestinal Cell Monolayers. *Nutrients* **2019**, *11*, 2271.
(36) Ching, S. H.; Bansal, N.; Bhandari, B. Rheology of Emulsion-Filled Alginate Microgel Suspensions. *Food Res. Int.* **2016**, *80*, 50−60.
(37) Fernández Farrés, I.; Douaire, M.; Norton, I. T. Rheology and Tribological Properties of Ca-Alginate Fluid Gels Produced by Diffusion-Controlled Method. *Food Hydrocolloids* **2013**, *32*, 115−122.
(38) Liétor-Santos, J. J.; Sierra-Martín, B.; Fernández-Nieves, A. Bulk and Shear Moduli of Compressed Microgel Suspensions. *Phys. Rev. E* **2011**, *84*, No. 060402.
(39) Lee, K. Y.; Mooney, D. J. Alginate: Properties and Biomedical Applications. *Prog. Polym. Sci.* **2012**, *37*, 106−126.
(40) H Muller, R.; Shegokar, R.; M Keck, C. 20 Years of Lipid Nanoparticles (SLN & NLC): Present State of Development & Industrial Applications. *Curr. Drug Discovery Technol.* **2011**, *8*, 207−227.
(41) Porter, C. J. H.; Trevaskis, N. L.; Charman, W. N. Lipids and Lipid-Based Formulations: Optimizing the Oral Delivery of Lipophilic Drugs. *Nat. Rev. Drug Discovery* **2007**, *6*, 231−248.
(42) Anton, N.; Benoit, J.-P.; Saulnier, P. Design and Production of Nanoparticles Formulated from Nano-Emulsion Templates-A Review. *J. Controlled Release* **2008**, *128*, 185−199.
(43) Shepherd, S. J.; Issadore, D.; Mitchell, M. J. Microfluidic Formulation of Nanoparticles for Biomedical Applications. *Biomaterials* **2021**, *274*, No. 120826.
(44) Fathordoobady, F.; Sannikova, N.; Guo, Y.; Singh, A.; Kitts, D. D.; Pratap-Singh, A. Comparing Microfluidics and Ultrasonication as Formulation Methods for Developing Hempseed Oil Nanoemulsions for Oral Delivery Applications. *Sci. Rep.* **2021**, *11*, No. 72.
(45) Anderluzzi, G.; Lou, G.; Gallorini, S.; Brazzoli, M.; Johnson, R.; O'hagan, D. T.; Baudner, B. C.; Perrie, Y. Investigating the Impact of Delivery System Design on the Efficacy of Self-Amplifying Rna Vaccines. *Vaccines* **2020**, *8*, 212.
(46) Spalinger, M. R.; Sayoc-Becerra, A.; Ordookhanian, C.; Canale, V.; Santos, A. N.; King, S. J.; Krishnan, M.; Nair, M. G.; Scharl, M.; Mccole, D. F. The JAK Inhibitor Tofacitinib Rescues Intestinal Barrier Defects Caused by Disrupted Epithelial-Macrophage Interactions. *J. Crohn's Colitis* **2021**, *15*, 471−484.
(47) Sala, G.; de Wijk, R. A.; van de Velde, F.; van Aken, G. A. Matrix Properties Affect the Sensory Perception of Emulsion-Filled Gels. *Food Hydrocolloids* **2008**, *22*, 353−363.
(48) Del Gaudio, P.; Colombo, P.; Colombo, G.; Russo, P.; Sonvico, F. Mechanisms of Formation and Disintegration of Alginate Beads Obtained by Prilling. *Int. J. Pharm.* **2005**, *302*, 1−9.
(49) Augustine, R.; Ashkenazi, D. L.; Arzi, R. S.; Zlobin, V.; Shofti, R.; Sosnik, A. Nanoparticle-in-Microparticle Oral Drug Delivery System of a Clinically Relevant Darunavir/Ritonavir Antiretroviral Combination. *Acta Biomater.* **2018**, *74*, 344−359.
(50) Giri, T. K.; Bhowmick, S.; Maity, S. Entrapment of Capsaicin Loaded Nanoliposome in PH Responsive Hydrogel Beads for Colonic Delivery. *J. Drug Delivery Sci. Technol.* **2017**, *39*, 417−422.

https://doi.org/10.1021/acs.biomac.3c00260
Biomacromolecules XXXX, XXX, XXX−XXX